Demonstration of Ultrahigh-Strength Nanocrystalline Copper Alloys for Military Applications

Project Number: WP-2139

Performing Organization

US Army Research Lab, Aberdeen Proving Ground

Principal Investigator:

Dr. Kris A Darling

Date
1/22/2012

Version
1

REPORT DOCUMENTATION PAGE

Form Approved
OMB No. 0704-0188

PLEASE DO NOT RETURN YOUR FORM TO THE ABOVE ORGANIZATION.

1. REPORT DATE *(DD-MM-YYYY)*	2. REPORT TYPE	3. DATES COVERED *(From - To)*
1-26-2012	Final	Dec 2010 - Dec 2011

4. TITLE AND SUBTITLE

Demonstration of Ultra High-Strength Nanocrystalline Copper Alloys for Military Applications

5a. CONTRACT NUMBER

5b. GRANT NUMBER

5c. PROGRAM ELEMENT NUMBER

6. AUTHOR(S)

Kris Darling, Suveen Mathaudhu and Laszlo Kecskes

5d. PROJECT NUMBER

WP-2139

5e. TASK NUMBER

5f. WORK UNIT NUMBER

7. PERFORMING ORGANIZATION NAME(S) AND ADDRESS(ES)

U.S. Army Research Laboratory
RDRL-WMM-F
APG, MD 21005

8. PERFORMING ORGANIZATION REPORT NUMBER

9. SPONSORING/MONITORING AGENCY NAME(S) AND ADDRESS(ES)

Strategic Environmental Research and Development Program
901 North Stuart Street, Suite 303
Arlington, VA 22203

10. SPONSOR/MONITOR'S ACRONYM(S)

SERDP

11. SPONSOR/MONITOR'S REPORT NUMBER(S)

12. DISTRIBUTION/AVAILABILITY STATEMENT

Approved for public release; distribution unlimited.

13. SUPPLEMENTARY NOTES

14. ABSTRACT

The objective of this research was to explore a novel alloy development via powder processing combined with innovative consolidation methodologies to fabricate laboratory-scale parts made from nanocrystalline Cu-Ta based alloys with thermal stability, ultra high-strength and hardness, and wear properties suitable for substitution for Cu-Be applications. Specifically, high-energy ball milling was used to fabricate non-toxic nanostructured Cu-Ta based alloy powders with a unique ability to retain their ultra high-strength properties to temperatures nearing the melting point of the Cu alloy.

15. SUBJECT TERMS

Nanocrystalline, Cu-Ta, Cu-Be, powder processing

16. SECURITY CLASSIFICATION OF:			17. LIMITATION OF ABSTRACT	18. NUMBER OF PAGES	19a. NAME OF RESPONSIBLE PERSON
a. REPORT	b. ABSTRACT	c. THIS PAGE			Kris Darling
UNC	UNC	UNC	UU		19b. TELEPHONE NUMBER *(Include area code)* 410-306-0862

Reset

Table of Contents

List of Figures

List of Tables

List of Acronyms

ABD: Acute Beryllium Disease
ACGIH: American Conference of Governmental Industrial Hygienists
ARDEC: Armament Research, Development and Engineering Center
ARL: Army Research Lab
ASTM: American Society for Testing and Materials
CBD: Chronic Beryllium Disease
DOD: Department of Defense
DOE: Department of Energy
DSC: Differential Scanning Calorimetry
ECAE: Equal Channel Angular Extrusion
EDS: Energy Dispersive Spectroscopy
EELS: Electron Energy Loss Spectroscopy
ESTCP: Environmental Security Technology Certification Program
FAST: Field Assisted Sintering Technology
FIB: Focused Ion Beam
GB: Grain Boundary
GS: Grain Size
HP: Hot Pressing
IACS: International Annealed Copper Standard
IARC: International Agency for Research on Cancer
MA: Mechanical Alloying
MA: Mechanical Alloying
MD: Molecular Dynamics
MWM: Meandering Winding Magnetometer
OSHA: Occupational Safety and Health Administration
PLS: Pressure-Less Sintering
SEM: Scanning Electron Microscope/Microscopy
SERDP: Strategic Environmental Research and Development Program
SPD: Severe Plastic Deformation
SPS: Spark Plasma Sintering
STEM: Scanning Transmission Electron Microscope/Microscopy
TEM: Transmission Electron Microscope/Microscopy
USNRC: United States National Research Council

Key Words

Cu-Be Replacement, Nanocrystalline, Cu-Ta, Copper Beryllium, Copper Tantalum, Powder Processing

Acknowledgements

The development of these Cu-Ta alloys was accomplished with assistance from the following individuals:

Anthony Roberts of the U.S. Army Research Laboratory

Joe Paras of the Army REDECOM-ARDEC, Picatinny Arsenal, NJ

Micah Gallagher of the U.S. Army Research Laboratory

Tim Frolov of George Mason University

David Foley of Texas A&M University

Brady Butler of the U.S. Army Research Laboratory

Prof. Yuri Mishin of George Mason University

Deepak Kapoor of the Army REDECOM-ARDEC, Picatinny Arsenal, NJ

Brad Klotz of the U.S. Army Research Laboratory

James Catalano of the U.S. Army Research Laboratory

James Paramore of the U.S. Army Research Laboratory

Abstract:

The objective of this research was to explore novel alloy development via powder processing combined with innovative consolidation methodologies to fabricate laboratory-scale parts made from nanocrystalline Cu-Ta based alloys with thermal stability, ultrahigh strength and hardness, and wear properties suitable for substitution for Cu-Be applications. Specifically, high-energy ball milling was used to fabricate non-toxic nanostructured Cu-Ta based alloy powders with a unique ability to retain their ultrahigh strength properties to temperatures nearing the melting point of the Cu alloy. It must be also mentioned that the as-milled powder particles had a mean diameter of approximately 100μm, but with an internal nanocrystalline microstructure, thereby removing the potential hazards associated with nanoscale particulate operations and handling.

The outcome of this project is fully successful, that is a viable material has been generated which can replace and compete with Cu-Be alloys.

The successful implementation of fabricating the Cu-Ta alloy powders into bulk parts was based on a novel approach for alloy design. The conventional methodology to prevent grain growth in nanocrystalline systems is to fight the equilibrium tendencies of grain growth by kinetically pinning the grain boundaries in place. However, by selectively choosing interfacially segregating solutes, the driving force for grain growth can be attenuated. That is, the magnitude of the collective grain boundary free energy can be reduced or potentially even negated, thereby placing the system into a deep, metastable state, preventing the growth of grains at any temperature. This thermodynamic concept, as employed in the Cu-Ta system, is elucidated by extensive experimentation and atomistic simulations.

The proof-of-concept for thermodynamic stabilization was validated, as powder processing was transferred from a laboratory scale to a larger pilot scale production. Within 8 months, powder processing was taken from a SPEX mill producing a few grams a day to a Zoz mill producing 1000g a day. This allowed the fabrication of parts to go from 3mm to over 70mm in dimensions. Two types of consolidation techniques were attempted: Field Assisted Sintering Technology (FAST) and Equal Channel Angular Extrusion (ECAE) both of which resulted in fully dense bulk parts.

It was also demonstrated that both the mechanical properties as well as the electrical properties of the Cu-Ta alloys can be tailored by changing the Ta content or by changing the temperature used during consolidation, **to match or exceed the properties of Cu-Be alloys**. We are currently able to provide much larger samples. However, this capability is outside the scope of the given effort. The consolidation techniques were primarily chosen to ensure successful production of bulk parts using methods which are scalable to larger parts while being representative of lower cost, high volume manufacturing.

This funded effort has resulted in two patent applications: one on the alloy composition and the other on the scale-up and part fabrication methodology. Additionally, results have been published in a high quality peer reviewed journal (Acta Mat.).

Project Objective:

The objective of this project was to explore novel alloy development via powder processing synergistically using innovative consolidation methodologies to fabricate laboratory-scale nanocrystalline Cu-Ta based alloys with better thermal stability, ultrahigh strength and hardness, and wear properties suitable for substitution in Cu-Be applications. Specifically, high-energy ball milling was used to fabricate nanostructured Cu-Ta based alloy powders with the unique ability to retain their ultrahigh strength properties to temperatures nearing the melting point of the Cu-Ta based alloy. Because of their high temperature stability, the powders may be consolidated to full theoretical density by using commercially viable consolidation techniques. Success to date has mitigated many of the risks associated with further development of these alloys. This is because nanocrystalline metals are one of the few, if any, metallic materials capable of competing with the extreme property set of Cu-Be alloys. **However, until now, no one has produced a nanocrystalline metal which exhibits such extreme stability that it can be readily formed and bulk consolidated at reasonable processing temperatures.** Additionally, the family of alloys is very low in toxicity and can be produced using commercially viable production and processing routes.

Background:

Current Status of CuBe Alloys

The dermatological, pulmonary, and systemic toxicity of Be and Be containing alloys has been known for over 70 years [1] and has been linked to a number of severe industrial health issues in the United States. During the past few years, medical research has continually lowered the threshold of Be which is known to adversely affect the human body. Attention has shifted from the immediate manifestations of high Be exposure demonstrated by Acute Beryllium Disease (ABD) to the more subtle, long term effects of Be sensitization and Chronic Beryllium Disease (CBD). Reduced lung function, pulmonary granulomas, and enlarged cardio vascular organs are just a few of the epidemiologic manifestations of CBD [2]. Furthermore, the International Agency for Research on Cancer (IARC) lists Be as a Category 1 carcinogen. While the Occupational Safety and Health Administration (OSHA), US Department of Energy (DOE) and the American Conference of Governmental Industrial Hygienists (ACGIH) have recommended that the acceptable exposure limit be lowered by as much as a factor of 40 [3], the United States National Research Council (NRC) has recommended that Be exposure be limited to "the lowest feasible level," as the agency's research could not establish any safe level of exposure [3].

The largest US utilization of Be is in Be containing alloys of which Cu-Be alloys are the most ubiquitous. Recent studies have shown that Cu alloys containing less than 4% Be have been linked to causing CBD, making them just as hazardous as the pure Be metal [4,5]. Due to the associated hazards of processing this material, the NRC has recommended that the Department of Defense (DOD) eliminate as many job tasks as possible that involve the exposure to Be products [6]. The development of alternative copper alloys with similar or greater physical properties without the adverse ecological and toxicological effects would therefore greatly reduce the health risks, liability and long term costs associated with manufacturing.

The main difficulty in replacing Cu-Be alloys lies in the outstanding physical properties of this material. The addition of 2 wt% Be can increase the strength of Cu six fold. Cu-Be alloys

exhibit high ductility, strength, elastic modulus, and demonstrate outstanding wear resistance. After precipitation hardening, these alloys are capable of achieving a tensile strength of 174 ksi (1200 MPa) while retaining a ductility of 7% elongation before failure. Equally important are the outstanding formability characteristics of these same alloys. Typically, a solution heat treated Cu-Be alloy can achieve 47% elongation with a yield strength of only 14.5 ksi (224 MPa) [7]. In addition, the Cu-Be class of alloys are easily machined and welded. These alloys are commonly found in applications where parts are subjected to severe forming conditions in the manufacturing process, but a high degree of strength is required in the final product. Some of the more prominent applications include: springs, bushings, valves, pumps, firing pins, electrical relays, navigational equipment, and non-sparking tools. This outstanding versatility leads to an exceptional performance and manufacturability that have only recently been outweighed by the health hazards associated with these materials.

Nanocrystalline Metals, a Suitable Alternative Replacement Material?

In recent years, nanocrystalline metals and alloys have had the attention of the scientific community. This is mainly due to the intriguing mechanical properties with which they are associated. Numerous reports now exist, indicating an order of magnitude increase in strength is possible in metals and alloys that exhibit grain sizes approaching the lower limit of nanocrystallinity [8-11]. While achieving high strength has never been a problem, the ability to achieve any amount of uniform elongation, the prerequisite for appreciable ductility, was a challenge in the past [12-14]. Recently numerous reports of improved ductility indicate that tens of percent elongation may be possible in nanocrystalline metals [15-17]. The combination of ultra high strength and improved ductility of nanocrystalline metals makes what was impossible in the past possible today, such as the replacement of Cu-Be alloys. However, as indicated by thermodynamic principles, nanocrystalline microstructures in metals are universally subject to coarsening at low homologous temperatures [18-23]. The result of such nano-to-micro scale coarsening is the loss of the remarkable physical properties and deformation behaviors associated with these microstructures. This inherent thermal instability severely limits the overall processing and applications of nanocrystalline metals. That is, nanocrystalline materials must be thermally stabilized if they are to be used in large-scale applications.

Theory on Stabilizing Nanocrystalline Metals for CuBe Replacement

The surface to volume ratio in nanocrystalline materials (i.e., with grain sizes < 100nm) increases rapidly, resulting in a large fraction of atoms occupying energetically unfavorable interfacial positions. The natural tendency of such a system is to seek a configuration which allows for the lowest possible energy construct. In pure elemental nanocrystalline materials this minimization of the system's overall energy is universally accomplished by the removal of excess interfacial area via grain growth. However, in binary systems, there exist other possible configurations which will allow for the minimization of the system's energy to take place other than by grain growth. One such configuration comes about by the interaction of the interfacial area with structural defects such as large substitution solutes. This interaction can be expressed by the Gibbs-Duhem equation for the adsorption of solute at an interface [24]

$$-SdT + Ad\gamma_b + n_i\, d\mu_i = 0 \qquad (1)$$

Here S is the interfacial entropy, A interfacial area, n_i the number of moles of solute at the interface, μ_i chemical potential of the solute at temperature T, and γ_b is the interfacial free

energy. At constant temperature the interfacial energy can be expressed as given by equation 2. The absorption of solutes to an interface, i.e., a positive interfacial excess (Γ) will, therefore, lower the energy associated with that interface.

$$d\gamma_b = -\frac{n_i}{A} d\mu = -\Gamma d\mu \tag{2}$$

Alternatively, the dependence of interfacial energy/grain boundary energy (γ_b) on solute segregation can be expressed as equation 3.

$$\gamma_b = \gamma_o + \Delta H_{seg} \frac{n_b^{seg}}{A} \tag{3}$$

γ_o is the intrinsic grain boundary free energy of the pure matrix, ΔH_{seg} is the enthalpy change due to grain boundary segregation of the solute and n_b^{seg} is the number of moles of solute on grain-boundary area A (the sign convention here is that $\Delta H_{seg} < 0$ if the energy is lowered and heat is evolved upon segregation).

Additionally, work by Weissmuller [24] proposed that, by using a simplified McLean approximation, a polycrystalline material undergoing grain growth at elevated temperatures should be treated as a closed system. If the interfacial area is in equilibrium with respect to the segregated solute atoms, and a change (dA) in grain boundary area is carried out reversibly at constant temperature and pressure, the total free energy change of the system is

$$dG = \gamma_b dA \tag{4}$$

Therefore, if solute segregation results in a value $\gamma_b = 0$, the associated free energy change dG = 0 and the resulting system will remain in an equilibrium. Further analysis shows that this is a minimum as opposed to a maximum in the free energy and, therefore, a metastable equilibrium state is achieved with respect to the grain-size stability. In essence, it can be reasoned that substitutional solutes act as the fulcrum point for the minimization of the systems' energy. If the interaction of a solute with an interface leads to a reduction in the overall energy of the system, then an increase in the solute excess of that interface will occur. The amount of solute accommodated in the excess grain boundary area of nanocrystalline alloys can be extensive, far above that predicted by equilibrium phase diagrams. Furthermore, the very act of grain growth necessitates the loss of occupied absorption sites. If grain growth is to occur, the re-absorption of solute from the grain boundaries back into the lattice will require an increase in the systems energy. Thus, the system is at a local minimum and any change in the configuration of the system results in an increase in the total energy. This buffering effect is the basis of the thermodynamic mechanism for grain size stabilization in nanocrystalline alloys. Nanocrystalline systems in such an equilibrium state are advantageous as the increased thermal stability allows for sintering of powders and/or forging of bulk objects at high temperatures while maintaining the exotic mechanical and physical properties. The ability to form a bulk material that retains the nanostructure is primarily dependent on the thermal stability of the material. In many cases the nanocrystalline substructure actually improves the sinterability of the material, but the sintering process results in such drastic increases in grain size that the resulting material is no longer nanocrystalline. It is precisely this reason that the

thermodynamically stable alloys are so appealing for producing bulk nanostructured materials. Improvements in thermal stability can open a regime of processing conditions that could allow full densification and the retention of a nanocrystalline structure.

Putting Theory into Practice, Creating a Stabilized Nanocrystalline Metal by High Energy Mechanical Alloying

High Energy Mechanical Alloying

Mechanical Alloying (MA) is a very versatile method for producing nanocrystalline metal and alloyed powders. In general, mechanical milling/alloying produces nanostructured materials with grain sizes <<100 nm by mechanical attrition of coarser-grained materials.

Advantages of Mechanical Alloying Over Other Processes

In general, there are three reasons that mechanical alloying was selected for production of the alloys proposed here over other methods.

1. Production of Particulates

Most metals/alloys can be prepared through mechanical-alloying with the product being in particulate form. In instances where materials are too ductile to be directly milled into powder as in the case of Cu, surfactants and/or cryogenic milling can be used to induce the production of powder. Fine particulates offer greater versatility when considering up- scaling to industrial manufacturing. This is due to the ability for these particulates to be sintered into almost any shape or size given the proper conditions (high temperatures and pressures) and is already a very long existing practice in the manufacturing scheme.

2. Increased Solubility Limit

High energy ball milling has been shown to vastly increase the limit of solid solubility in many metallic systems in which equilibrium room temperature solubility does not otherwise exist. In general, many solvent-solute systems that exhibit large changes in enthalpy upon segregation (a prerequisite for a large reduction in interfacial energy) are systems which exhibit very little solid solubility in each other. Thus, high energy ball milling has the ability to create supersaturated solid solutions.

3. Production of the Smallest Possible Grain Size

High energy ball milling is known to dramatically reduce the grain size in metallic systems to less than 10 nm which is not possible in other sever plastic deformation processes (SPD). Other methods such as electroplating use solute as a surfactant to reduce the grain size and thus require high weight percents, as much as 15-20 wt% to reduce the grain size [25-28]. In mechanical alloying, the grain size reduction comes from the mechanical energy, as such, the addition of a solute is only needed to stabilize, not refine the grain size, and therefore can be added in much lower quantities 0.1-10at%.

Challenges with Consolidation of Nanocrystalline Materials

The phenomenal material properties predicted by the Hall-Petch relationship generated a push to produce finer and finer grain sizes and structures over the past five decades. Within recent years, a great deal of work has focused on the issues of producing nanocrystalline powders; however, the development of functional engineering components requires these nanostructures to be consolidated into fully dense macroscopic structures. Many researchers have reported on the enhanced sintering characteristics of nanostructured materials [29,30] that allow high densities to be achieved at much lower temperatures than their coarse grained counterparts. Equation (5) describes a multi-stage sintering model developed by Johnson et al.[31] that relate the normalized densification rate of the specimen ($d\rho/\rho dt$) to the grain size (G).

$$-\frac{d\rho}{3\rho dt} = \frac{\gamma\Omega}{kT}\left(\frac{\Gamma_V D_V}{G^3} + \frac{\Gamma_b \delta D_b}{G^4}\right) \tag{5}$$

where γ is the surface tension, Ω is the atomic volume, k is Boltzmann's constant, T is the absolute temperature, Γ_v and Γ_b are density dependant constants that describe the microstructure, and δ is the grain boundary thickness. As described above, reducing the grain size of the sample can increase the densification rate exponentially. Unfortunately, both grain growth and densification are driven by the same diffusion based mechanisms. Therefore, the thermal instabilities that lead to an enhanced densification rate also increase the rate of grain growth in this material and the microstructure of the material after sintering is no longer nanocrystalline. The decoupling of grain growth and densification is essential for producing bulk specimens which are useful for most engineering applications[32].

Consolidation of Thermally Stable Powders

Microstructures that exhibit thermal stability in their grain structure also tend to exhibit a similar stability for their particle structure. Sintering is a process that depends on the reduction of energy from the high energy state of the finely divided powder to the lower energy of the fully consolidated product. Much of the driving force that leads to densification is based on the overall reduction in surface area. Thermodynamically stable materials are created by reducing the grain boundary and surface energies so that they are essentially the same as that of the bulk material; therefore, the driving force for densification is reduced in the same manner that the driving force for grain growth is inhibited. When examining equation (5), the microstructure scaling and surface energy terms are highly dependent on the interfacial energies associated with the system and directly influence the densification behavior of the material.

Although the thermal stability of these materials tends to inhibit the sinterability of nanostructured materials under conventional conditions, improvements in thermal stability can open a regime of processing conditions that allow full densification and the retention of a nanocrystalline structure for more novel consolidation approaches. In particular, the application of external pressure during the sintering process, as practiced in Hot Pressing (HP) and Field Assisted Sintering Technology (FAST); or a combination of pressure and shear, as demonstrated by equal channel angular extrusion (ECAE), can greatly improve the tendency for densification.

Pressure Assisted Sintering

Hot pressing techniques have demonstrated commercial viability in consolidating metal powders for a number of decades[33]. Hot pressing is typically carried out by heating a uniaxial press during the forming process. The addition of external pressure can cause plastic yielding which can reduce the sintering temperature and time significantly while achieving the same density in the final product[34-36]. In the Field Assisted Sintering Technology (FAST) process, a high current is passed through the die assembly creating a plasma between particles during the sintering process. The plasma generated during this process has been shown to clean the surfaces of particles by volatilizing contaminants and thereby improving interparticle connectivity, which is of prime importance during the initial stages of sintering. Furthermore, this highly localized heating method can increase the heating rate drastically, which helps to inhibit surface diffusion and strain relaxation processes that reduce the overall driving force for densification. As a result, full density can be reached at lower temperatures and much shorter heating times while requiring minimal pre-processing.

Severe Plastic Deformation Processing

Recent demonstrations of novel processing methods involving temperature, high shear *and* high pressure have shown promise for bonding high strength particulate materials[37-39]. The ECAE process subjects a billet to high shear around an "L" shaped channel. ECAE can be performed at elevated temperatures for any number of passes and the billet can be rotated between passes to provide precise texture control for the material. This method, which induces Severe Plastic Deformation (SPD) at elevated temperatures, has demonstrated its effectiveness in consolidating powders that have a very narrow processing window and cannot be easily consolidated using conventional methods such as high hardness, brittle metallic glass powders. The addition of high shear can significantly reduce the temperature required to achieve full density and allow the consolidation of metastable microstructures[39]. Another benefit of these SPD methods is that the material samples retain the same basic geometry and cross-section as the starting piece, thus allowing for relatively simple scale-up.

Experimental Methods:

Downselection of Alloys

Based on thermodynamics, a host of solutes were selected to provide increased thermal stability, see Figure 1 below. Figure 1 shows the effect of different solutes on lowering the interfacial energy associated with Cu grain boundaries as a function of the interfacial concentration. After some preliminary milling trials, the Cu-Ta system was chosen as the system to demonstrate significant stability, thereby holding the most promise for facilitating the production of bulk parts with a nanocrystalline microstructure.

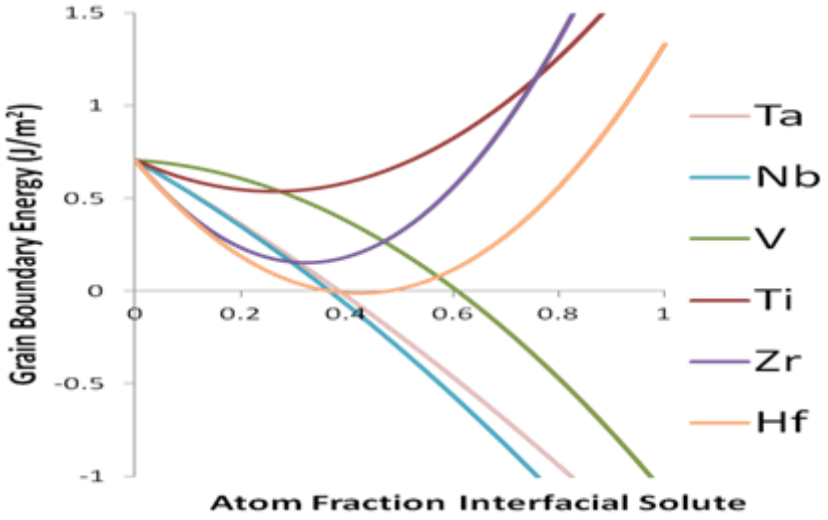

Figure 1. The effect of select solutes on reducing the interfacial energy in nanocrystalline Cu as a function of the interfacial solute content.

The available latitude in thermal stability permitted a significantly wide temperature window for a combinatorial approach concurrently using pressure, temperature and possibly shear. As such, we used a two-pronged approach to consolidate these materials to full density. The first approach used a common conventional industrial practice to consolidate these materials using pressure-less sintering (PLS). However, the thermal stability was so great that pressure-less sintering was not an option for bulk consolidation. The second set of methods relied on newer technologies like FAST or high temperature ECAE processing. These methods produced bulk fully dense parts without the need for the use post-consolidation hot forging or rolling. It should be mentioned that these approaches provide pathways to the necessary scale-up and are both capable of producing near net shape components that greatly reduce process costs by limiting subsequent machining operations.

From a toxicology perspective, Ta is not a hazardous substance or preparation according to EC-directives 67/548/EEC or 99/45/EC and their various amendments and adaptations and, therefore, makes it a suitable alloying addition. Additionally, it is not listed by the IARC (International Agency for Research on Cancer), NTP (National Toxicology Program), OSHA (Occupational Safety for Health Administration), ACGIH (American Conference for

Governmental Industrial Hygienists) or EU (European Union). Ta has also been readily used in clinical application for over 50 years.

Laboratory Investigations: Small Powder Quantity

Hardened steel vials and 440C stainless steel balls were used for mechanical alloying in a SPEX 8000M shaker mill. Milling was accomplished by loading the hardened steel vials with Cu and Ta powders (~ 325 mesh, 99.9% purity) to produce the desired compositions Cu with 10 and/or 1 at% Ta. A ball-to-powder ratio of 10:1 with a powder charge of 5 g was loaded into the vials. Vials were sealed in an argon atmosphere glove box with less than 1 ppm oxygen and H_2O concentration prior to milling. Mechanical alloying in the SPEX 8000 shaker mill was performed at liquid nitrogen temperature for 8 hours. This was accomplished by flowing liquid nitrogen continuously around the steel Mechanical milling resulted in un-agglomerated powders with a particle size range of 20-100 μm. Small preform tablets were made by uniaxially pressing the as-milled powder at 3.5 GPa in a 3 mm diameter tungsten carbide die. These samples were subsequently annealed for 4 hours at various temperatures under pure H_2 gas.

Laboratory Investigations: Transition from Small to Large Scale Powder Quantity

Upon successful fabrication of Cu-Ta alloys at ARL, process scale-up was conducted in conjunction with ARDEC, who is uniquely equipped with a suite of powder processing equipment. Mechanical alloying via high energy milling was utilized on a scale 10-20X larger than SPEX milling through attrition milling. This effort utilized a 2 liter unit, but the process is readily scalable, as an 8 liter unit already exists at ARDEC. If larger amounts of powder are desired in the future, 20 and 100 liter Zoz units are available from the equipment manufacturer. Figure 2 shows examples of the SPEX and Zoz mills used in the transition to larger scale powder production.

There is a large difference in how these mills operate which mainly affects the deformation mechanisms involved in the alloying process and grain size refinement. Zoz mills are considered to have slightly lower energy than SPEX mills, however, they can be easily scaled to accommodate industrial powder production levels. (This required new optimizations in milling practice which have not yet been completed). For example, materials produced by high energy cryogenic milling had a higher initial hardness of 5GPa as compared to the Zoz milled powder being closer to 4GPa. That is, the cryogenically milled powder retained a higher hardness at any given processing temperature. It should be mentioned that ARL does have a large scale cryogenic attritor mill, modeled after large scale cryogenic mills currently used in industry. However, within the scope of this proposal, this alternate processing route was not investigated, but will be an intergral part of the full proposal. Future efforts will include process parameter and alloy composition optimization . Figure 3 shows difference before and after milling using the Zoz mill. Figure 3 (Right Image), shows the high degree of mixing which can be attained using the Zoz mill, where the light gray tantalum, and dark grey copper are homogenously dispersed on a fine scale. However, Figure 3 (Right Image) also shows that the Zoz milling procedure is not yet optimized as complete mix has not occurred. Figure 4 gives an example of the powder produced using the Zoz milling process and an example of the consolidated geometries produced from the powders using the FAST technique.

Figure 2. Demonstration of the process scale up going from gram quantity milling (left) to hundreds of grams (right).

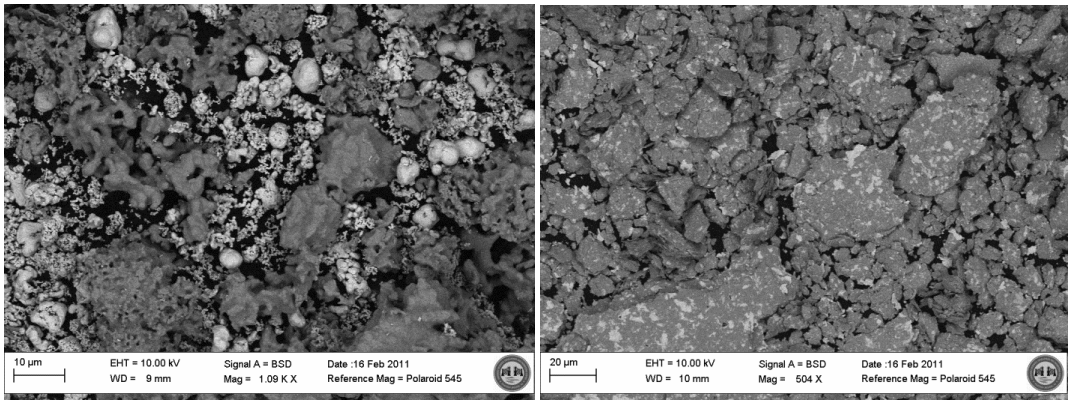

Figure 3. Microstructure of the Cu-Ta system before (left) and after (right) mechanical alloying using the Zoz mill.

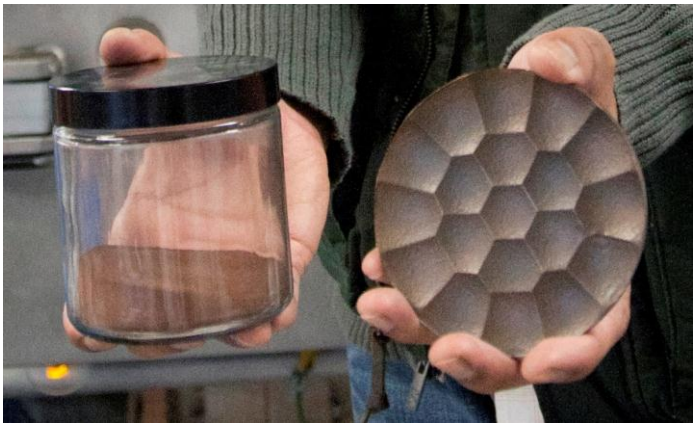

Figure 4. Examples of Cu-Ta powders processed using a Zoz mill and a FAST consolidated part.

Laboratory Investigations: Consolidation Methods

Currently, ARL has a small scale ECAE press, capable of extruding ¾-inch by 9-inch long bars. The small scale cryogenic mill (SPEX mill) was used to produce several hundred grams of powder for processing through the ECAE press. As such, specimens labeled as ECAE processed have been consolidated using powders originating from the small scale cryogenic mill. In contrast, all samples labeled as FAST processed, have been consolidated using powder originating from the Zoz mill.

Equal Channel Angular Extrusion (ECAE)

ECAE consolidation experiments were carried out as follows, the as milled powder was placed into a bore hole (12.5 mm in diameter and 100-130 mm long) in a nickel billet (25.4 mm X 25.4 mm 200 mm) and sealed in an argon atmosphere (O_2 < 1 ppm). Prior to ECAE, the die assembly was heated to (475^{o}C). The nickel cans, loaded with the Cu-Ta powder, were heated to a range of temperatures (600-900^{o}C) prior to extrusion. The equilibrated cans were then quickly dropped into the die and the extrusions performed. The temperature of the can immediately prior to extrusion was monitored by thermocouples: one of which was located on the backside of the can in the center of its length; and the other was placed in the center of the can 10 mm from the bottom. A single-pass extrusion through a channel angle of 90^o was performed at the respective temperature with an extrusion rate of 25.4 mm/s (1 in/s). The process was repeated three additional times for a total of 4 passes through route B_c. Route B_c entails a 90^o rotation between successive passes around the long axis of the ECAE can. The extracted specimen revealed a fully consolidated sample with no evidence of prior particle boundaries and 0% porosity. The density of the consolidated samples was determined by using Archimedes principle. Processing diagram 1 shows a general flow process for the steps involved in processing of Cu-Ta powder into bulk consolidated pieces using the ECAE technique. First, milled powder is loaded into metal cans, these cans are then inserted into the ECAE die and extruded around a 90^o angle this process is repeated until the powder is consolidated into bulk fully dense part, which is encased in the nickel can, (shown in the bottom left image). Currently consolidated pieces can be 0.5inch in diameter and about 9 inches long.

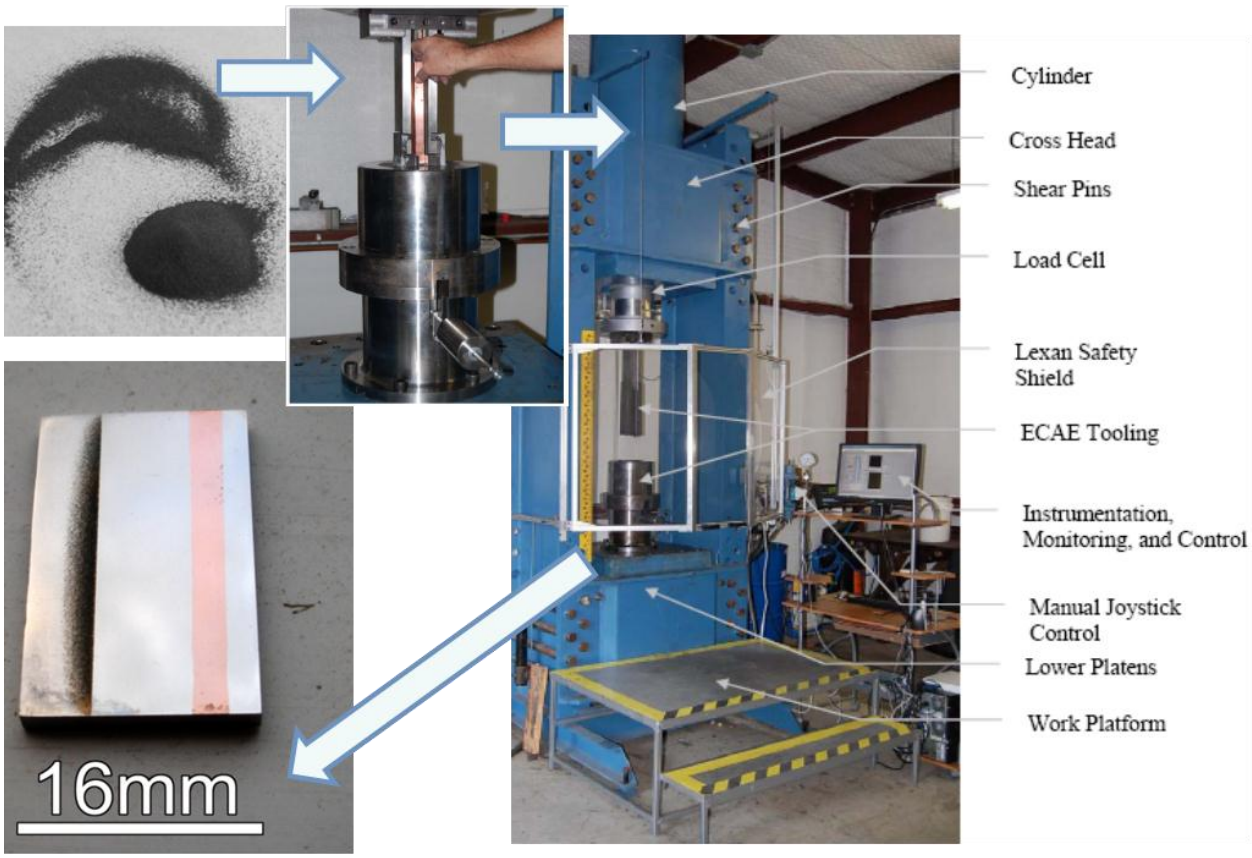

Processing Diagram 1: Steps showing the processing of the Cu-Ta alloys using the ECAE technique. Fully densified consolidates had hardness of 3.75GPa and a retained grain size of 30nm.

Field Assisted Sintering Technology (FAST)

Post mechanical alloying, the powders were consolidated using field assisted sintering, also known as spark plasma sintering (FAST/SPS). The system utilized at ARDEC is the FCT HP D 125, capable of producing plates up to 150mm in diameter, reaching temperatures up to 2400°C, and applying up to 125 tons of pressure. The sintering process is achieved by applying uniaxial pressure in conjunction with passing electrical current through powder loaded in a conductive die set (graphite). As a result of the electrical current, joule heating takes place and sintering times are drastically reduced – in a matter of minutes for this effort. Plates, approximately 40mm and 80mm in diameter, were consolidated using pressures up to 100MPa and temperatures up to 900°C. While full density can be achieved in as little as 4 minutes, sintering schedules with longer soak times were used to tailor the alloy microstructure and resultant properties. It is important to note that because the process relies on die sets, near-net-shaping can be done if the proper tooling is made for the process. Note, FAST/SPS is also limited in the thickness of parts that can be made. For this reason, future efforts will explore hot isostatic pressing (HIPing) and its associated process optimization for the fabrication of large parts.

Processing diagram 2 shows the steps involved in processing of Cu-Ta powder into bulk consolidated pieces using the FAST technique. In the FAST process, powders are loaded into graphite dies and compacted under uniaxial pressure. Next, the application of joule heating occurs by application of passing high current through the sample resulting in heating of the compact mass from the inside out. The FAST process typically yields bulk parts in simple geometries such as round or square plates. Within 12months we were able to move from the lab scale to fully dense large scale parts of various diameters having a retained nanocrystalline microstructure, and high hardness equal to current Cu-Be alloys

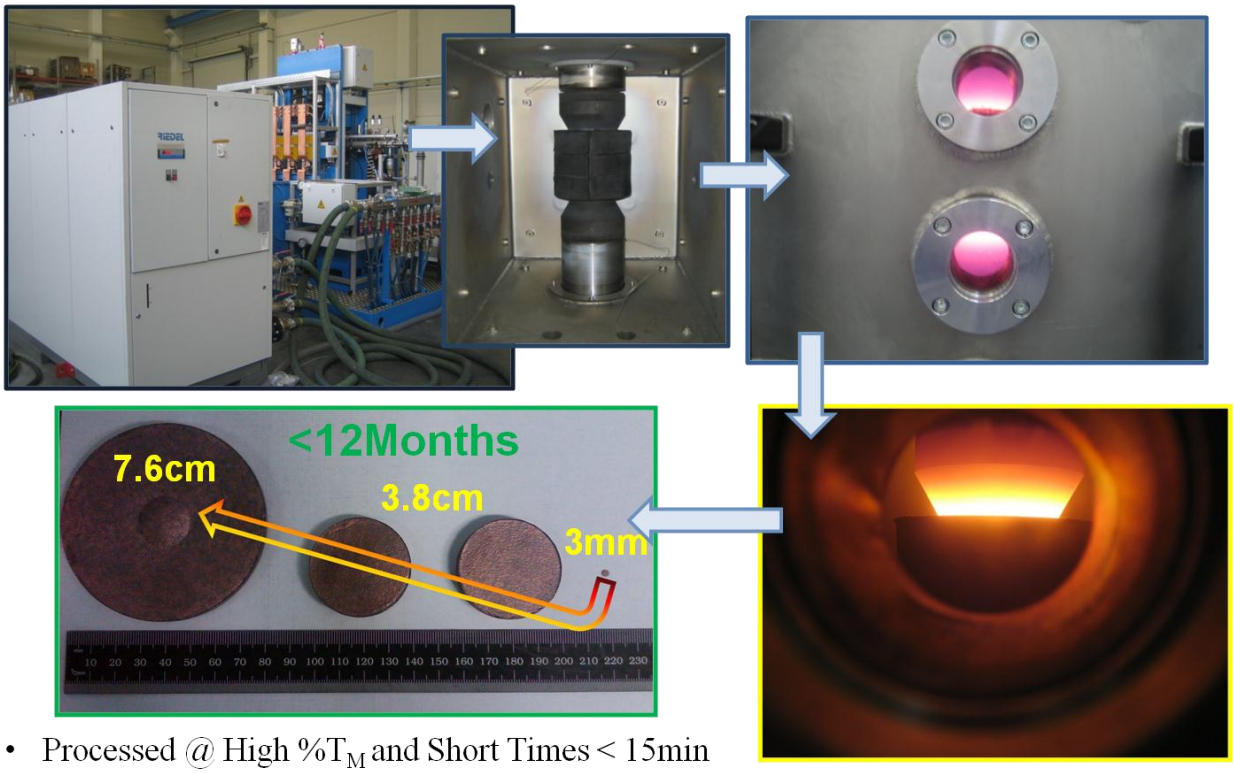

Processing Diagram 2: Steps showing the processing of CuTa alloys using the FAST technique. Because of the excellent thermal stability of the alloy powder, scaling from a 3- to a 76-mm diameter disk took place in less than 12 months.

Characterization of Alloy Properties

Vickers Hardness

Vickers hardness was used to determine the mean hardness associated with the as milled powder, heat treated samples, and post processed samples (FAST and ECAE). Tests were performed on ISO 9000 Certified equipment using ASTM standard operating procedures.

Compression Testing

Compression tests were performed as to ascertain the mechanical properties including: yield and ultimate compressive strength, ductility and toughness. These tests were conducted using various strain rates including:

Conventional Strain Rates: Strain rates were on the order of $1X10^{-4}$.

High Strain Rates: Strain rates were on the order of $3\text{-}6X10^{3}$. High strain rate studies were carried out on a Kolsky bar (or Split–Hopkinson pressure bar).

Wear Testing

Pin-on-disk wear testing was performed using an Implant Sciences Corp ISC-200 tribometer and a computer interface data acquisition unit, PC-stripchart. ASTM G99-05, "Standard Test Method for Wear Testing with a Pin-on-Disk Apparatus," was referenced during wear testing. The Cu-Ta disk samples were mounted on the top of the rotating platform of the tribometer. The MP35N steel pin samples, ½-inch in diameter x 1-1/2-inch length, were securely attached to a precision balanced lever arm, which was used to apply vertical loads to the pin. The load cell (force gauge) located on the top platform measured the loading force applied by the pin. This data was used to calculate the kinetic friction coefficient, which was recorded and displayed in real time by the software program. In order to begin testing, the pin was first contacted with the surface of the disk sample. The force gauge was then balanced before weight was added to the system. Testing commenced once parameters such as rotation speed, radius, and weight were set using the front panel parameter controls. All friction measurements were conducted without lubrication and in air. Finally, the results were analyzed using PC-stripchart and graphed via Microsoft Excel. Test parameters were: weight settings 500 and 900 grams, rotational speed 80 and 100rpm, duration 24 hrs.

Electrical and Thermal Conductivity

Electrical and Thermal Conductivity were made by using a Meandering Winding Magnetometer (MWM) and the conductivity is reported in %IACS. IACS stands for International Annealed Copper Standard. This standard is based on the conductivity of annealed copper to be (5.8001×10^{7} S/m) which is defined as 100% IACS at 20°C. All other conductivity values are defined relative to this conductivity standard. As an example, iron with a conductivity value of 1.04×10^{7} S/m, has a conductivity of approximately 18% of that of annealed copper and this is reported as 18% IACS. Conductivity values in Siemens/meter can be found by dividing the % IACS by the conductivity value of 1.7241×10^{-6}. Thermal conductivity was estimated by applying the Wiedemann-Franz Law.

Transmission Electron Microscopy (TEM), Focused Ion Beam (FIB), Electron Energy Loss Spectrometry (EELS), and Energy Dispersive Spectrometry (EDS):

TEM samples were produced using a dual beam FEI Nova Nano Lab 600. TEM imaging and analysis was carried out in a JEOL JEM 2100F. TEM analysis was used to image the lattice,

grain boundary, and interfacial structure and secondary phases. Chemical analysis was made possible by using electron energy loss spectroscopy (EELS) and energy dispersive x-ray spectroscopy (EDS) combined with advanced TEM/STEM. TEM samples were prepared using an in-situ lift-out method using a dual beam focused ion beam scanning electron microscope (FIB/SEM). In- situ sample preparation was used for producing site specific samples with few artifacts resulting from the preparation process.

Scanning Electron Microscopy (SEM) with Energy Dispersive Spectrometry (EDS)

SEM analysis was used to determine the spatial distribution and chemistry of phases, investigate hardness indentations, characterize residual porosity, and image fracture surfaces. SEM imaging of the samples was accomplished using a Hitachi S-4700 equipped with an EDS detector.

Differential Scanning Calorimetry Analysis (DSC)

DSC analysis was used to investigate the thermal response of the generated microstructure: including melting, and several exothermic events such as intermetallic formation, phase separation and grain growth as a function of temperature and heating rate. Differential scanning calorimetry experiments were performed in a Netzsch STA 409C equipped with a TASC 414/3 controller.

X-Ray Diffraction Studies

X-ray diffraction of the ball milled and annealed powders, as well as the bulk consolidated pieces was performed with an X'Pert PRO PANalytical MPD x-ray diffractometer using CuKα ($\lambda = 0.1542$ nm) radiation. The data collected consisted of crystallite size of the as-milled, heat treated, and bulk consolidated samples in addition to any secondary phases which were formed.

Atomic Simulations

Atomic simulations were performed as a way to corroborate the experimental findings. These methods are described in the results section.

Results:

Experimental Results: Small Scale Samples

Cryogenic milling produced a nanocrystalline composite. Scherrer grain size (GS) estimates of the microstructure length scale suggested the mean GS of the Cu matrix and that of the residual Ta particles were 6.7 and 6 nm, respectively. Upon further x-ray analysis, a small but prominent shift to lower angles was detected for the Cu fundamental reflections. Estimates of the lattice parameter, based on this shift suggested approximately 1-2at% Ta was forced into the Cu lattice. While 1-2 atomic percent is not a large increase in solubility, both theoretical and experimental evidence suggest this percent solute is more than sufficient to thermodynamically stabilize a nanocrystalline microstructure below 100 nm. The Vickers hardness of the as milled

powder was measured to be approximately 4.8 GPa. This value is double that reported for pure nanocrystalline Cu[15, 40-42]. It is suggested that the elevated hardness is a product of a much smaller GS, hardening due to fine nanoscale Ta particle dispersions and solid solution strengthening of the Cu matrix by oversized Ta atoms. Figure 5 summarizes the decrease in hardness versus annealing temperature for Cu-10at% Ta, high purity electroplated nanocrystalline Cu and conventional coarse-grained Cu. The difference in hardness between the samples is quite apparent. Cu-10at% Ta has an initial hardness which is greater than 10 times that of coarse grained Cu and maintains hardness values greater than as deposited electroplated nanocrystalline Cu even after annealing at 1040^{o}C for 4 hours. The annealing temperature of 1040^{o}C represents a homologous temperature equal to 3% below the melting point of Cu. Figure 6 gives a TEM bright field micrograph of the microstructure of Cu-10at% Ta after annealing at 1040^{o}C for 4 hours showing a mean GS of 166nm. In comparison, the electroplated Cu has a dramatic decrease in hardness and a rapid increase in GS to the micron scale within the first 300 degrees of annealing. This is not unexpected for pure nanocrystalline Cu as this temperature range is consistent with literature descriptions of the expected onset temperature for strain relaxation and grain growth[40, 43-50.]

Figure 7 is a composite image showing a collected DSC spectrum and TEM/SEM micrographs of the microstructure at congruent temperatures along the DSC signal trace. The figure was constructed by first performing a complete DSC run, which consisted of two separate heating events. Both were performed by heating the sample at a rate of 20 K/min from 24 to 950 ^{o}C. The second heating event was necessary to collect the base line, the difference between the two curves resulted in the given trace. Next, three separate experiments were accomplished by running the DSC up to and not over specified temperatures as outlined by prominent exothermic events along the given DSC trace, as labeled. This was done such that the characteristic microstructures would correlate with the observed exothermic events. These powders were then mounted and polished. SEM images were taken from the polished cross sections while TEM images were created by performing H-bar lift outs with a dual beam FIB and subsequent imaging in a TEM. TEM/SEM images for the highest temperature 1040^{o}C were taken from a compact annealed in a tube furnace. This was necessary as the high annealing temperatures resulted in unwanted reactions with the available DSC crucibles and atmosphere. The selected temperatures along the DSC trace are 540, 636, 770, and 1040 ^{o}C. The measured TEM GS for each annealing temperature were measured and found to be 20, 33, 57, and 166 nm respectively. The Ta particle size for each annealing temperature was also measured. The particle size for the first two temperatures were difficult to accurately measure in the SEM images, however, at 770 and 1040 ^{o}C, the mean particle size was determined to be 40 and 100 nm.

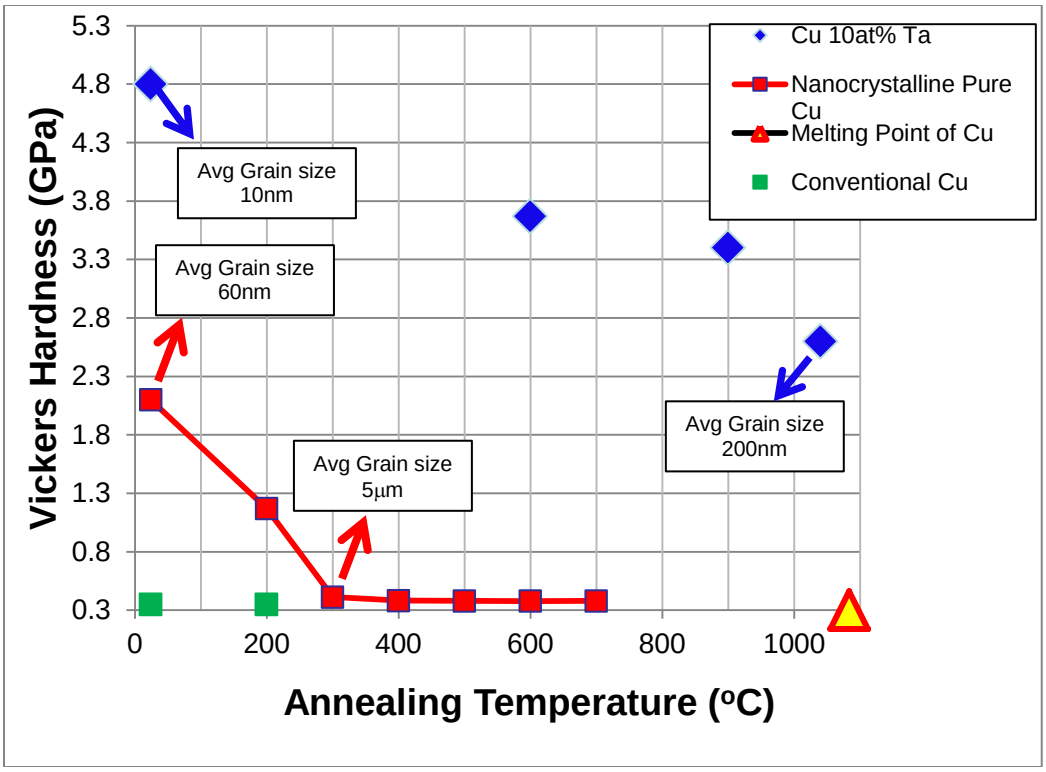

Figure 5. Plot showing the effect of Vickers hardness on annealing temperature for Cu-10 at% Ta, electroplated nanocrystalline Cu and conventional coarse-grained Cu.

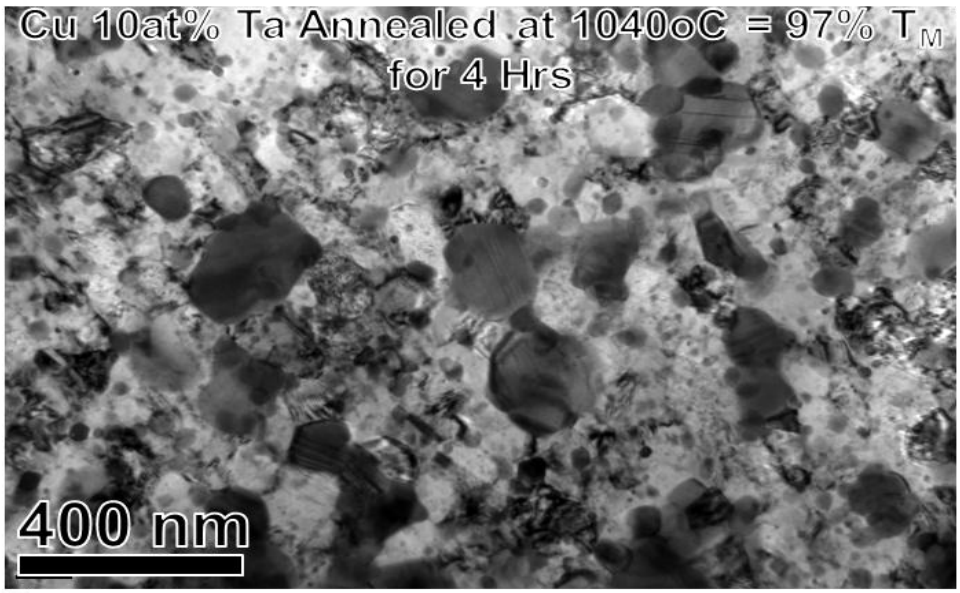

Figure 6. Bright field TEM Micrograph showing microstructure of Cu-10 at% Ta after having been annealed at 1040°C for 4 hours.

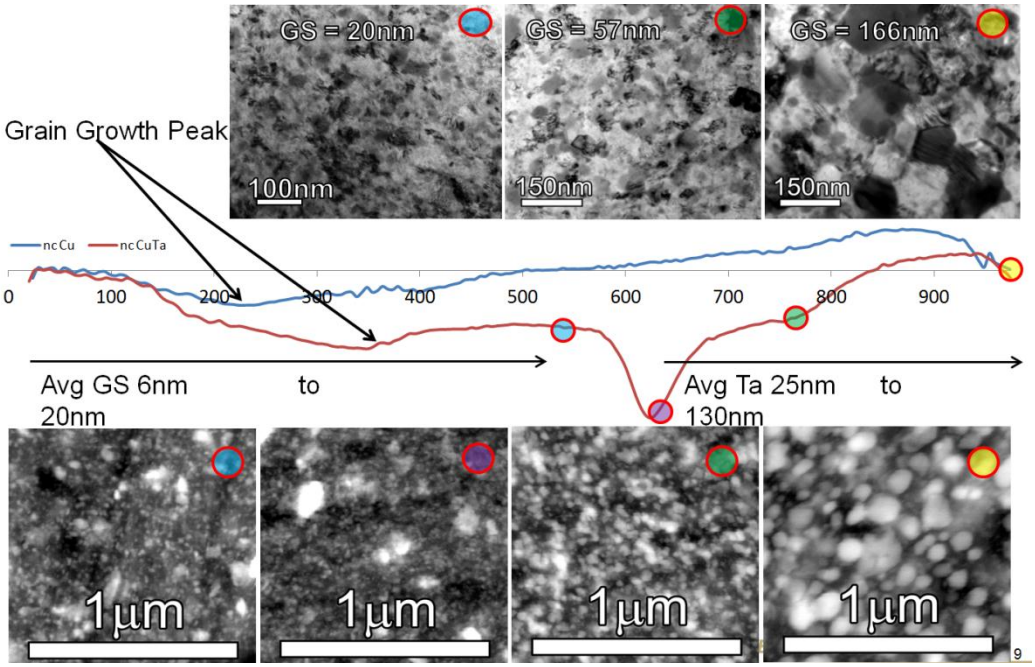

Figure 7. DSC curves with TEM and SEM micrographs showing the microstructural evolution as a function of temperature for Cu-10 at% Ta. The blue curve is a DSC trace for pure nanocrystlline Cu.

Figure 8a is a TEM bright field micrograph for Cu-10 at% Ta annealed for 4 hours at 900 ^{o}C (87%T_M). The microstructure is mainly composed of 75 nm copper grains with small regions exhibiting abnormal growth. The Ta particles were observed to have a trimodal size distribution, those of approximately 100nm, < 30 nm and in figure 8b those < 10nm in diameter. It can be seen in figure 8b that a number of the < 30 nm precipitates occupy GB positions. This type of distribution was generally observed over the entire microstructure. Figure 8c shows one of the smaller 7 nm precipitates. However to the left of the precipitate are several dark points of contrast where the signal is delocalized. Such contrast is indicative of atomic clusters in which the atomic number of those clusters are higher than the surrounding matrix. It can be said with some certainty that such spots are atomic clusters of Ta solute. In fact it has been theoretically predicted that such clusters are favorably formed in a self assembled nano scale liquid liquid emulsion of Cu-Ta [51]. Balling has been known to create supersaturated solids solution and in this case up to 2 at% Ta may have been force into solution. Thus at such high homologous temperatures it may be expected that our mechanically alloyed system of Cu and Ta may behave similarly to the observations made by Mishin et al. in a Cu-Ta liquid-liquid system[51].

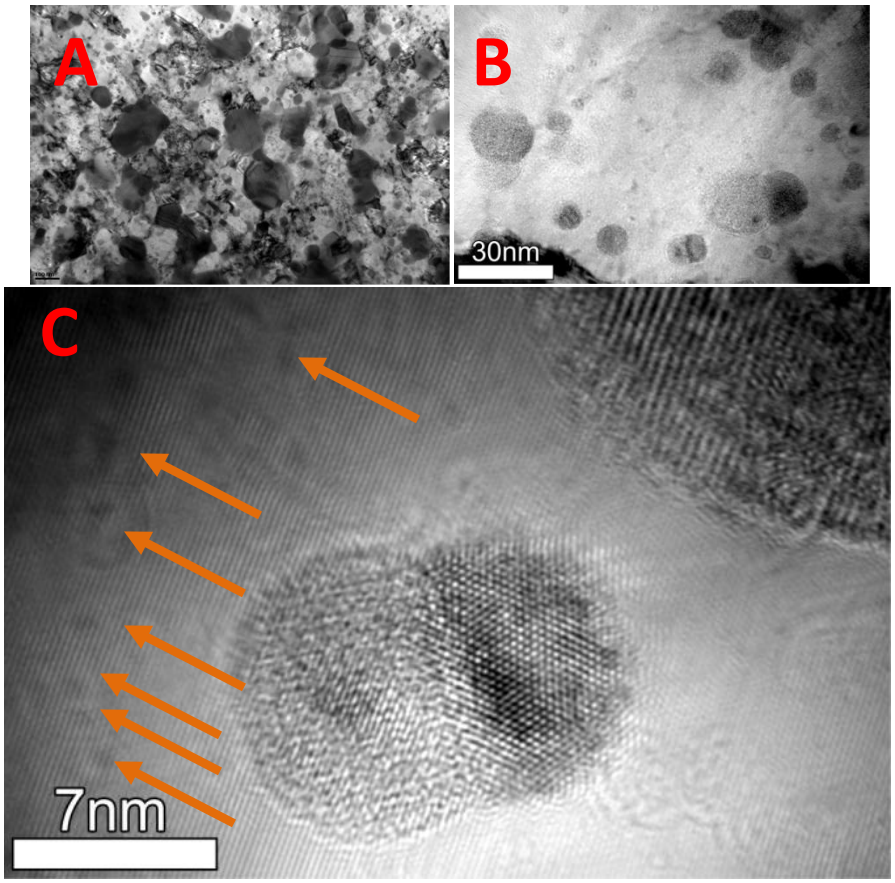

Figure 8(A-C). Bright Field TEM images showing the dispersion of both Ta particles and atomic clusters. Orange arrows point to possible atomic clusters of Ta.

Our recent work with modeling of nanocrystalline Cu with dissolved Ta in solution (discussed in the next section) shows that Ta solute has a dramatic effect on stabilizing nanocrystalline Cu. It was found that randomly distributed atoms of Ta had an effect of stabilizing the Cu matrix, however, once Ta atoms were place at the GBs, as in a GB segregated state, the microstructure resisted coarsening up to the melting point of Cu. As the temperature was increased up to the melting point the segregated Ta atoms which formed a continuous layer surrounding the grains broke and formed semi-continuous nanoscale emulsion within the GB region. The atomic clusters of Ta making up the GB emulsion prevented the grain growth up to the melting point. It can be concluded that such atomic clusters and GB pinning dispersoids add significant thermal stability and highly strengthen the microstructure.

Experimental Results: Simulations

The MD simulations were performed to model nanocrystalline samples representing experimental as-milled structures containing either pure copper or a Cu-6.5at.%Ta alloy with segregated and randomly distributed Ta solute. While the simulated time scales are not representative of experimental time scales, atomic simulations give a comparative difference between stability of the different microstructures. As mentioned two types of Ta distribution in the alloy were tested: a purely random distribution, and segregation at GBs, dislocations, and

other defects. In the second case, most of the Ta atoms were residing at GBs due to their large area. Structural stability of these materials was evaluated by a set of anneals at different temperatures. On the timescale of MD simulations, grain growth in pure Cu starts at temperatures of about $0.4T_M$ of Cu. This corresponds to even lower temperatures on the experimental timescale. Experiments indicate the onset of grain growth in polycrystalline Cu at temperatures between 420 K and 550 K, $(0.32\text{-}0.42)T_M$ of Cu. The introduction of Ta atoms causes a strong retardation of the grain growth. Even for a uniform distribution of Ta, the grains begin to grow at temperatures of about $(0.6\text{-}0.7)T_M$ of Cu. In the alloy with GB segregation, the Ta effect is truly remarkable. The pinning of GBs becomes so strong that the usual grain growth by capillary driven GB migration is not observed at any temperature up to T_M of Cu. Instead, as the temperature approaches T_M of Cu, the smallest grains melt and re-crystallize in a new crystallographic orientation continuing the orientation of a neighboring larger grain. It is this unconventional mechanism that eventually leads to coarsening of the structure and overall encapsulation of the Ta clusters inside the grains at temperatures above $(0.85\text{-}0.9)$ T_M of Cu. We expect that this mechanism should cease to operate as the grain size increases but this prediction is yet to be tested. The resistance to grain growth observed in the samples with uniform Ta distribution can be explained by additional dissipation due to the interaction of moving GBs with Ta atoms. At high temperatures and on experimental time scales, this interaction could lead to the formation GB segregation and thus retardation of GB motion by the solute drag effect[52–55]. On the other hand, when Ta segregation was created in the starting configuration, the GBs became completely pinned and practically did not move during the simulations. Figures 9-11 are snap shots from atomic simulations which graphically show the above results.

Figure 9 gives the initial (a) and final (b) structure of nanocrystalline Cu during a 10ns simulated anneal at 750K. The figure 9 atoms near grain boundaries and defects are colored yellow. In the final state after annealing only a few twin boundaries and dislocations remain.

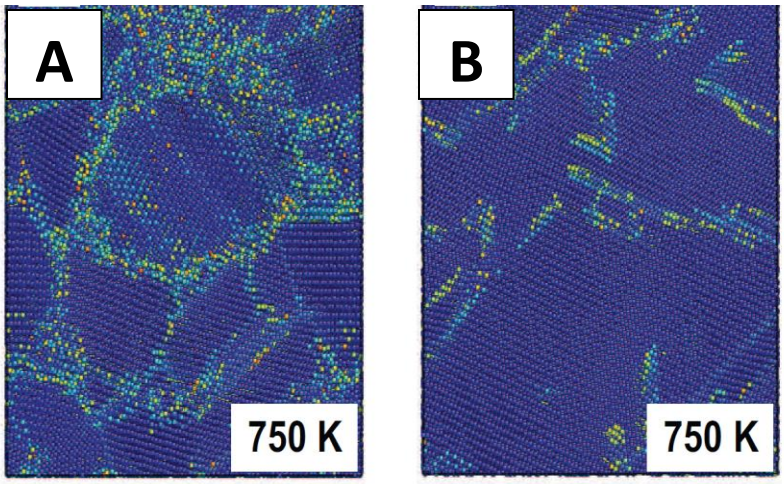

Figure 9. Simulation snap shots showing the microstructural evolution of pure nanocrystalline Cu at 750K.

Figure 10 gives the initial (a) and final (b) structure of nanocrystalline Cu having a uniform distribution of Ta atoms in the Cu matrix after a 24 ns long simulated anneal at 750 K and 1000 K. Here the presence of the Ta atom provides more thermal stability than pure nanocrystalline Cu.

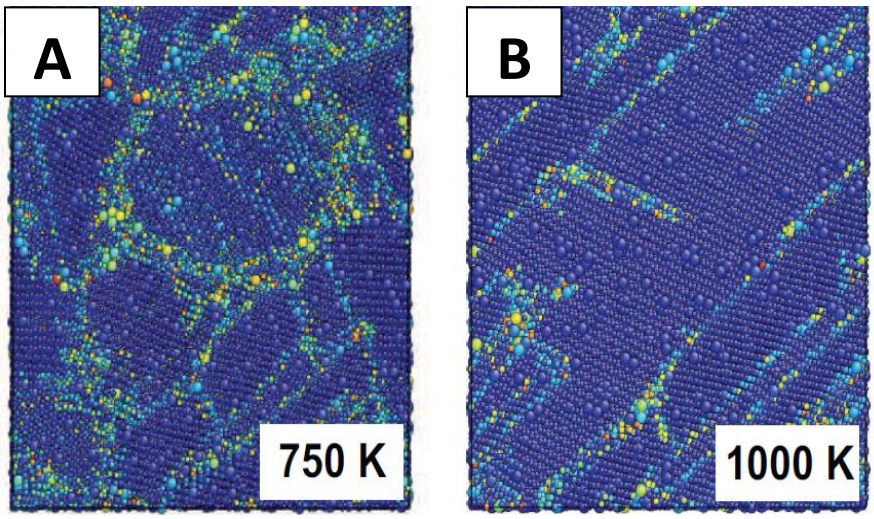

Figure 10 Final (a) and final (b) structures of nanocrystalline Cu having a uniform distribution of Ta after a 24 ns long simulated anneal at 750 K and 1000 K. Ta atoms are depicted here as larger spheres.

Figure 11 gives the final structures of nanocrystalline Cu having Ta atoms segregated to the grain boundaries in Cu after a 45 ns long simulated anneal at 1100 K (a) and 1200 K (b). Ta atoms are depicted as blue spheres Cu as gold. Here the presence of the Ta atom once segregated to grain boundaries provide more thermal stability than either pure nanocrystalline Cu or nanocrystalline Cu having a random distribution of Ta in the matrix.

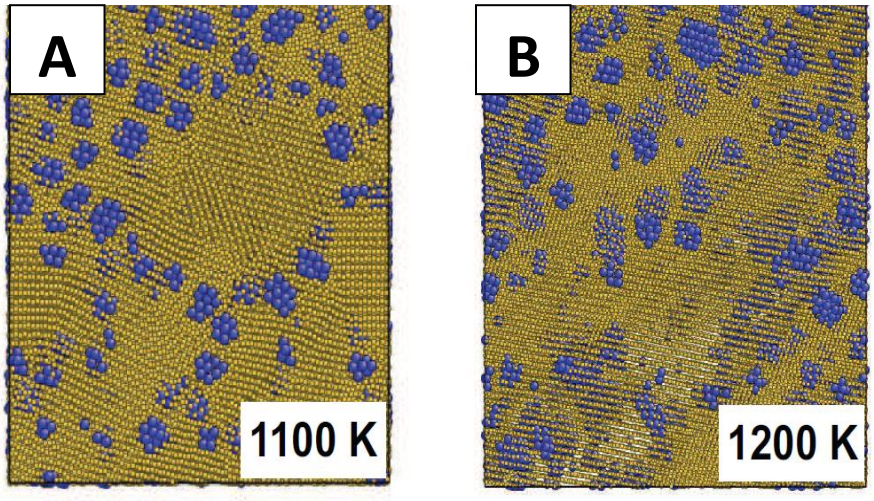

Figure 11 Final structures of nanocrystalline Cu having Ta atoms segregated to the grain boundaries in Cu after a 45 ns long simulated anneal at 1100 K (a) and 1200 K (b). Ta atoms are depicted as blue spheres Cu as gold.

Simulated tensile tests were performed to demonstrate the profound impact of Ta alloying on mechanical strength. As expected, it was found that the addition of Ta strongly increases the yield and flow stresses, especially when Ta is segregated at GBs or forms nano-clusters. Figure 12 shows the simulated tensile curves.

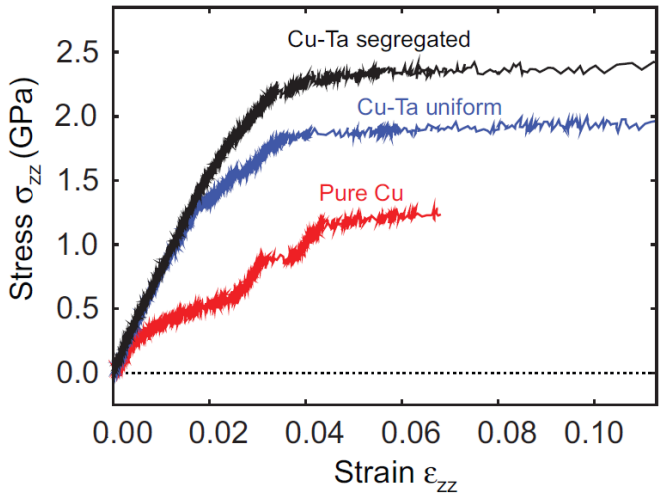

Figure 12. Stress-strain curves from simulated tensile test performed at 300 K for pure Cu, Cu-Ta having uniform segregated Ta solute and Cu-Ta having grain boundary segregated Ta solute.

Although detailed mechanisms of Ta segregation and nano-particle formation are not fully established, the following plausible scenario emerges from our simulations and recent experiments. During the ball milling, a certain percentage of Ta atoms are forced into the Cu lattice, with the remaining Ta forming separate grains. During the subsequent heat treatment, partial growth of copper grains occurs, along with dislocation rearrangements and other recovery processes. As the moving GBs and dislocations sweep through the lattice, Ta atmospheres form which eventually lead to GB segregation. An additional amount of Ta can be supplied to GBs by diffusion along dislocation lines (dislocation-enhanced diffusion[52]). As the material is annealed further, the super-saturated Ta segregation begins to form nano-clusters, a process which requires diffusion-controlled redistribution of Ta inside GBs. We emphasize that this processes is only possible due to the phenomenon of fast diffusion along GBs[52]; it could not occur in the Cu lattice where Ta diffusion is extremely slow even near the melting point of Cu. Since experiments show the formation of Ta particles with sizes of a few nanometers and larger, we assume that the nano-clusters eventually transform to larger particles, which then continue to grow by the Ostwald ripening mechanism.

Experimental Results: Mechanical Properties

Compression Results: High Strain Rates

Compression tests were performed on both the FAST and ECAE consolidated materials. Two types of compression tests were completed, conventional strain rates and high strain rates. Figure 13 gives the high strain rate compression tests for FAST consolidated Cu with 10at% Ta processed at elevated temperatures to full consolidation. The curves follow the conventional

trend, that is, rapid strain hardening within the first few percent of plastic strain followed by zero or strain softening afterward. The microstructure of the sample processed at 700 ^{o}C is finer, and therefore elicits a higher strength mechanical response. Additionally, due to the finer grain size, the material undergoes significant strain softening. This is contrasted by the data at 900^{o}C where the same material was processed at a higher temperature and for a longer time. In this case the yield stress is lower and the sample exhibits no strain softening in addition to showing more elongation. Figure 14 shows the high strain rate mechanical response for the ECAE consolidated materials. Here three stress strain curves are reported Cu-10 at% Ta processed at 700 ^{o}C and 900 ^{o}C and Cu-1 at%Ta processed at 700 ^{o}C. In comparison to the FAST samples, the ECAE samples have higher mechanical properties. This also agrees with the difference noted in hardness between the FAST and ECAE samples. When comparing the ECAE, samples differences are noted. The Cu-10 at% Ta processed at 700 ^{o}C is the highest strength sample, and exhibits a strong strain softening effect. Additionally, changing the processing temperature or composition has an effect on changing both the strength and ductility of the material.

If a comparison is made between the high strain rate tests and the simulated tensile tests a fair agreement is made.

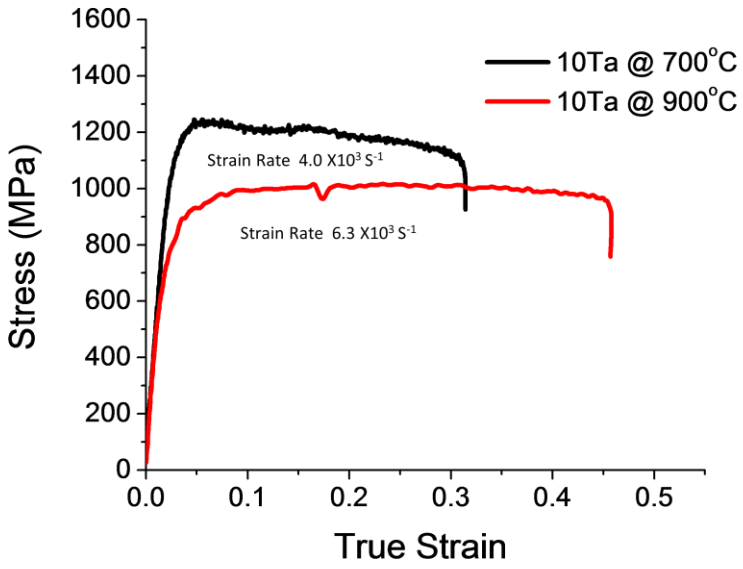

Figure 13. High strain rate stress-strain curves for FAST consolidated Cu-10 at%Ta processed at 700 and 900^{o}C.

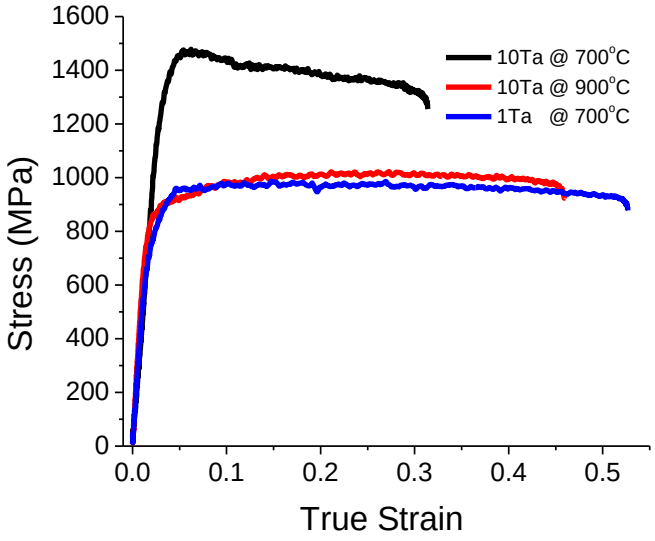

Figure 14. High strain rate stress-strain curves for EACE consolidated Cu-10 at%Ta processed at 700 and 900°C and Cu-1 at%Ta processed at 700°C.

Compression Results: Quasi-static Strain Rates

The general trends observed in the high strain rate tests are also observed at normal strain rates Fig 15 and Fig 16.

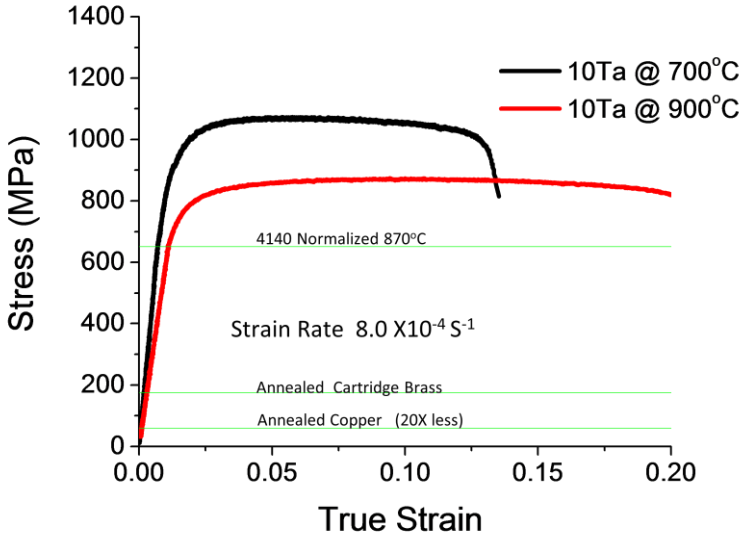

Figure 15. Conventional strain rate, stress-strain curves for FAST consolidated Cu-10 at%Ta processed at 700 and 900 °C. Showing comparative yield data for different materials process at similar temperatures.

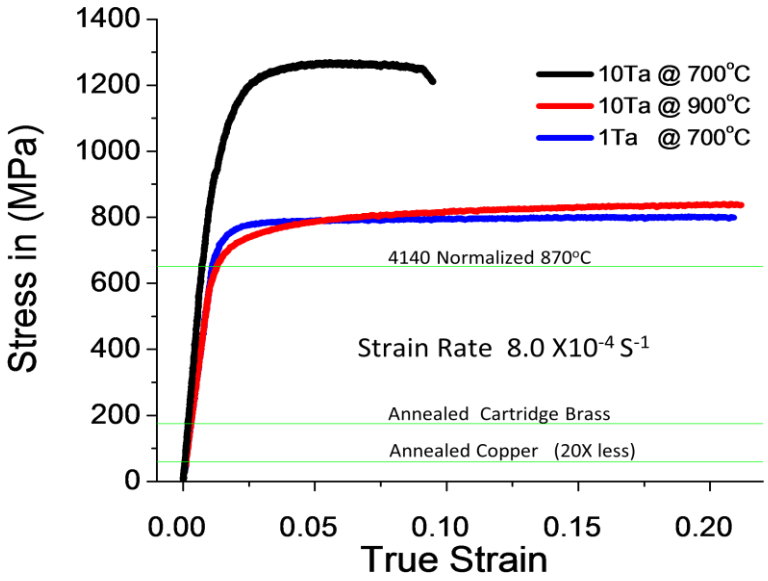

Figure 16. Conventional strain rate, stress-strain curves for ECAE consolidated Cu-10 at%Ta processed at 700 and 900 ^{o}C and Cu-1 at% Ta processed at 700 ^{o}C, showing comparative yield data for different materials processed at similar temperatures.

Wear Testing Results

Visually, both Cu disks exhibited the most wear of all the samples tested. The Cu disks displayed a significant amount of wear debris/particles depositing along the wear track, while little or no wear was shown across the steel disk. The Cu-Ta sample also experienced significant wear but much less than those seen in Cu samples. The lost mass and volume data (Table 1) further support these findings. Together, Cu disks lost more mass and volume than the Cu-Ta disks while the steel sample experienced negligible wear.

Friction profiles of both Cu disks observed in Figure 18 show a gradual increase in friction coefficient initially and then leveled off at 0.6. This is an indication that the samples wear at an increasing rate and then reach a relatively steady state toward the end of the testing. Both Cu 1 and 2 experienced comparatively high friction coefficients and this validates the severe wear seen in both samples. For Cu-Ta 1, the friction coefficient shows a continual increase throughout and reaches its max at 0.44 toward the end of the test run. As for the steel sample, its friction coefficient noticeably reached a steady state at 0.25 soon after the testing commenced. This distinct pattern might suggest that the steel sample was experiencing friction insufficient to cause wear and will likely withstand these test conditions longer than its counterparts.

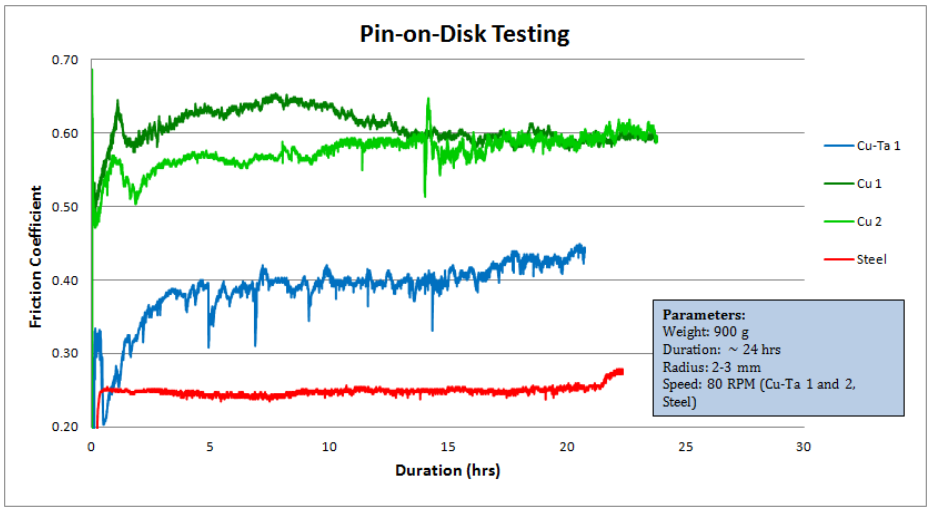

Figure 17. Wear test data for work hardened and annealed Cu, Cu-Ta processed by FAST and hardened D2 tool steel.

Table 1. Lost mass and volume at 900 g weight setting.

	Hardness (GPa)	**Mass Loss (mg)**	**Volume Loss (mm^3)**
D2 Tool Steel	7.0GPa	0.3	--
Cu-Ta 2	3.7GPa	4.2	0.58
Cu 2	1.1GPa	8.3	0.94
Cu 1	0.55GPa	6.3	0.81

Experimental Results: Electrical and Thermal Conductivity

The electrical and thermal conductivity measurements were performed on both the FAST and ECAE consolidated materials. Figures 19 and 20 give the resultant data. Figure 19 reports the electrical conductivity along with the hardness and sample type (FAST/ECAE). The general trend is revealed, that being, the harder/finer the microstructure the lower the conductivity. The complete data set falls within the conductivity of pure copper and pure aluminum and remains constant as a function of frequency or depth into the bulk sample. The same trend holds for the calculated thermal conductivity (Figure 20). All samples have values well within the range of Cu-Be alloys.

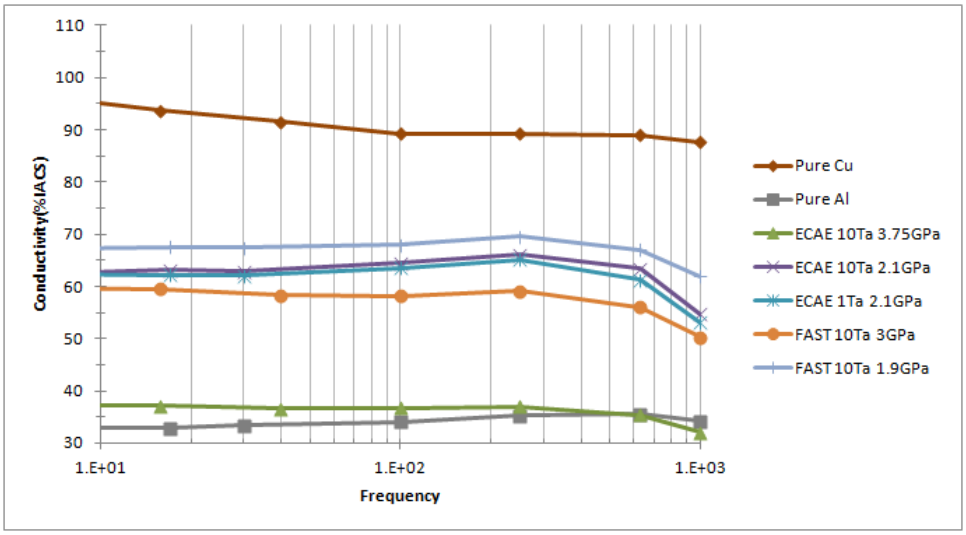

Figure 18. Electrical conductivity data for consolidated FAST and ECAE samples, the hardness and comparative Al and Cu standards are given for comparison.

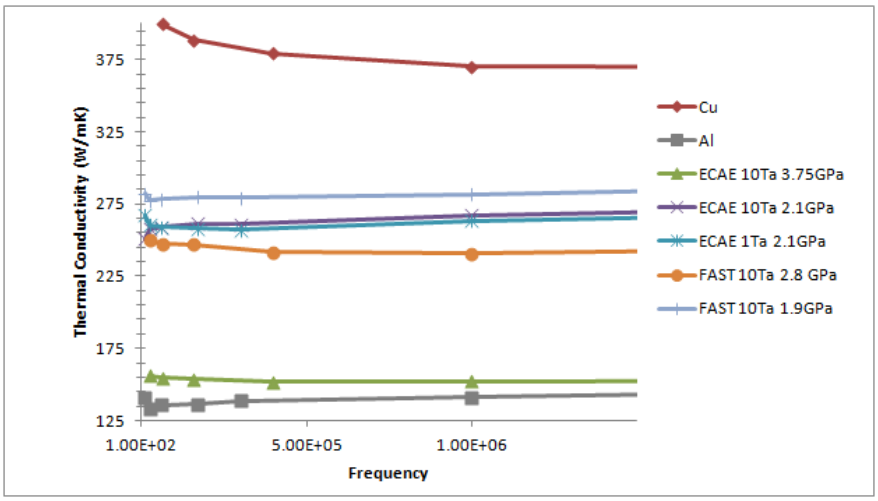

Figure 190. Thermal conductivity data for consolidated FAST and ECAE samples, the hardness and comparative Al and Cu standards are given for comparison.

Conclusions:

A host of characterization techniques were used to study and develop a new family of nanocrystalline alloys based on the Cu-Ta binary system. These alloys, designed using advanced thermodynamic concepts, have extreme high temperature stability, thereby allowing the retention of advanced mechanical properties in fully consolidated powder-based parts. Fabrication of large-scale bulk specimens has been successfully demonstrated. The physical underpinnings for the behavior of these alloys were elucidated by extensive experimentation and atomistic simulations. That is, the nonequilibrium processing provided by high energy ball milling creates a metastable solid solution between two immiscible element (Cu and Ta). Upon heating and decomposition, Ta atoms collect at grain boundaries and form atomic clusters which eventually coarsen to larger dispersoids. The combined effect of lowered grain boundary energy and stable dispersoids freezes the microstructure at the nanoscale thereby facilitating consolidation by forging at higher temperatures. **The potential success of the alloyed Cu-Ta powder is demonstrated in the ability to rapidly fabricate useful parts having equivalent or better properties than those of Cu-Be alloys or any other currently used Be replacement alloys**. Application of both the FAST and ECAE consolidation techniques resulted in fully dense bulk parts. Geometries include rods and plates with near net shaped designs.

It was also demonstrated that both the mechanical properties as well as the electrical conductivity properties can be tailored by changing the Ta content or by changing the temperature used during consolidation to match or exceed the property envelope of Cu-Be alloys. We are currently at the cusp of providing much larger samples, however, this task was outside the scope of the given effort. Note, the consolidation techniques selected were chosen to ensure successful production of bulk parts using methods conducive to both scaling to larger parts and lower cost high volume manufacturing and this will be the focus of future work. It is also important to note that these alloys could be easily processed or produced by other non equilibrium processing methods to give rise to other advanced applications. For example, both physical vapor deposition and or cold/thermal spraying could be used to generate high hardness and highly temperature resistant coatings. This is because it is the chemistry that drives the stability and thus, the mechanical properties.

Comparison of Alloy Properties

Table 2 below gives a comparison of the measured properties of the Cu-Ta alloys as compared to Cu-Be alloys. **Results reflect that Cu-Be properties can be achieved in a Be-free alloy**.

Table 2. Comparison of Cu-Be and Cu-Ta Properties.

	Ultimate Strength (GPa)	**Yield Strength (GPa)**	**Elongation (%)**	**Hardness (GPa)**	**Electrical Conductivity (% IACS)**	**Thermal Conductivity (W/mK)**	**Density (g/cm^3)**
CuBe Alloys	0.4 - 1.4	0.4 - 1.3	1 - 60	0.6 - 4.4	15 – 60	103 - 242	8.4 – 8.9
CuTa Alloys	0.6 – 1. 3	0.6 – 1.1	10 – 25	1.8 – 5.0	40 – 70	150 - 280	8.9 - 10

We have shown in the seed project that using a combination of novel powder processing and innovative consolidation methodologies (i.e., FAST and ECAE), laboratory-scale thermally stable nanocrystalline alloys with ultrahigh strength, hardness, and wear properties suitable for substitution in Cu-Be applications could be made. That is, for the first time, high-strength Cu-Be properties could be achieved in a Be-free alloy. While significant gains in the fundamental understanding of bulk thermally stable nanomaterial properties were made, a number of scientific and technological gaps still exist. Some of these include:

1. Effect of Ta concentration over the range of 0.01 to 10 at.% Ta. As the solute concentration controls or influences both the grain size and distribution of Ta dispersoids, it will also control and alter all the physical and mechanical properties allowing further room to tailor and optimize alloy properties. This is because it is the alloy chemistry that drives thermal stability and, thus the mechanical and physical properties.

2. Effect of FAST and ECAE processing parameters (pressure, temperature, or time) of product properties. While some of the physical properties were characterized, a great deal more could be accomplished, including an extensive analysis of tensile, compressive, and shear properties, at low and high temperatures, as well as a function of the strain rate. Additionally, fatigue and wear resistance should also be addressed.

3. Transition to a high-volume, large-scale manufacturing environment. Aspects of manufacturability, including, scalability of both powder and part production, as well as the quality and reproducibility of manufactured parts should be investigated. Feasibility of more advanced processing should be equally assessed, including, machining and joining of as-fabricated parts. Lastly, while the majority of work has focused on the high-energy mechanical alloying and consolidation of powders using high temperate forging operations, other types of manufacturing have been overlooked.

4. It is also important to take note of the fact that these alloys could be processed or produced by other non-equilibrium processing methods for other advanced coating applications. For example, both physical vapor deposition and or cold/thermal spraying could be used to generate high hardness and high-temperature resistant coatings.

References:

1. M.E. Kolanz, Applied occupational and environmental hygiene, 2001. 16(5): 559-567.
2. H. Vainio, and J.M. Rice, Journal of Occupational and Environmental Medicine, 1997. 39(3): 203.
3. Committee on Beryllium Alloy Exposures, committe on Toxicology, National Research Council. Washington DC: The National Academies Press , 2008.'
4. G.A. Day, et al., International archives of occupational and environmental health, 2006. 79(2): 161-164.
5. CNN. "Nearly 2,000 People Warned of Possible Beryllium Exposure ." 2009 http://www.cnn.com/2009/HEALTH/01/29/los.alamos.beryllium/index.html accessed Jan 31, 2010

6. "NRC urges minimal Beryllium Exposure". Chemical & Engineering News 86 (33): 26. 18 Aug. 2008.
7. E.A. Brandes, Smithells metals reference book. 6th ed. 1983: Butterworths London.
8. M.A. Meyers, A. Mishra and D.J. Benson. Prog. Mat. Sci., 51, 2006, 427.
9. K.S. Kumar, H. Van Swygenhoven and S. Suresh. Acta Mat., 51, 2003, 5743.
10. C.C. Koch and J. Weertman In: Nanostructured materials. Norwich: Noyes Publications, 2002. Pg. 393.
11. J.R. Weertman, D. Farkas, H. Kung, M.Mayo, R. Mitra and H. Swygenhoven., MRS Bull, 24, 1999, 44.
12. C.C. Koch, Scripta Mat., 49, 2003, 657.
13. E. Ma, Scripta Mat., 49, 2003, 663.
14. Y.T. Zhu and X. Liao, Nature Mat., 3, 2004, 351.
15. K.M. Youssef, R.O. Scattergood, K.L. Murty, J.A. Horton and C.C. Koch., Appl. Phys. Lett., 87, 2005, 091904-1.
16. K.M. Youssef, R.O. Scattergood, K.L. Murty and C.C. Koch., Scripta Mat., 54, 2006, 251.
17. Y. Zhao, X. Liao, S. Cheng, E.Ma and Y.T. Zhu., Adv. Mater., 18, 2006, 2280.
18. H. Gleiter, Progress in Mater. Sci., 33, 1989, 223.
19. R. Birringer, Mater. Sci Eng. A., 33, 1989, 117.
20. B. Gunther, A. Kumpmann and H.D. Kunze. Scripta Mater., 833, 1992, 27.
21. G. Hibbard, K.T. Aust, G. Palumbo and U. Erb. Scripta Metall., 44, 2001, 513.
22. U. Klement, U. Erb, A.M. ElSherik and K.T. Aust., Mater. Sci. Eng. A., 203, 1995, 177.
23. T.R. Malow, C.C. Koch., Acta Mat., 45, 1997, 2177.
24. J. Weissmuller, NanoStructured Mater., 3,1993, 261.
25. A.J. Detor, C.A. Schuh, Acta Mat., 55, 2007, 371.
26. A.J. Detor, C.A. Schuh, Acta Mater 55, 2007, 4221.
27. A.J. Detor, J.K. Miller, C.A. Schuh, Philos Mag., 86, 2006, 4459.
28. A.J. Detor, C.A. Schuh, J Mater Res., 22, 2007, 3233.
29. W. H. R., Journal of the American Ceramic Society, 64(1), 1981, 19.
30. R.A. Andrievski, , International journal of powder metallurgy(1986), 30(1), 1994, 59.
31. J.D. Hansen, R.P. Rusin, M. Teng and D.L. Johnson, Journal of the American Ceramic Society, 75(5), 1992, 1129.
32. J.R. Groza and R.J. Dowding, Nanostructured Materials, 7(7), 1996, 749.
33. W. Chang, et al., Nanostructured Materials, 4(5), 1994, 507.
34. J.R.Groza, Journal of Materials Engineering and Performance, 2(2), 1993, 283.
35. F. Ren, A. Chandra, and V. Tvergaard, Journal of Manufacturing Science and Engineering, 120, 1998, 349.
36. J.R. Groza and A. Zavaliangos, Materials Science & Engineering A, 287(2), 2000, 171.
37. K.T. Hartwig, H. Zapata, A. Parasiris and S.N. Mathaudhu, in ”Powder Materials: Current Research and Practices”, edited by F.D.S Marquis, N.N. Thadhani and E.V. Barrera, TMS Publishing, (2001), 211-221.
38. D. Canadinc, H.J. Maier, M. Haouaoui and I. Karaman, ”Scripat Mat.” 58 (2008), 307.
39. S.N. Mathaudhu, K.T. Hartwig and I. Karaman, “J. Non-Crys. Solids” 353 (2007) 185.
40. J. Eckert, J.C. Holzer, C.E. Krill III, W.L. Johnson., J. Mater. Res., 7, 1992, 1751.
41. Y. M. Wang, K. Wang, D. Pan, K. Lu, K. J. Hemker, E. Ma., Scripta Mat., 48, 2003, 1581.

42. Y.F. Shen, L. Lu, Q.H. Lu, Z.H. Jin, K. Lu., Scripta, Mat., 52 , 2005, 989.
43. Y.K. Huang, A.A. Menovsky, F.R. de Boer., Nano Struct. Mat., 2, 1993, 587.
44. L. Lu, L.B. Wang, B.Z. Ding, K. Lu., Mat. Sci. Engr. A, 286, 2000, 125.
45. L. Lu, M.L. Sui, K. Lu., Acta Mat., 49 (2001) p. 4127.
46. H.J. Fecht, E. Hellstern, Z. Fu, W.L. Johnson., Metall. Trans. A, 21A, 1990, 2333.
47. L. Lu, N. R. Tao, L.B. Wang, B.Z. Ding, K. Lu., J. Appl. Phys., 89, 2001, 6408.
48. H. Jiang, Y.T. Zhu, D.P. Butt, I.V. Alexandrov, T.C. Lowe., Mat. Sci. Engr. A, 290, 2000, 128.
49. Y. Zhang, N.R. Tao, K. Lu., Acta. Mat., 56 (2008) p. 2429.
50. K.B. Yin, Y.D. Xia, C.Y. Chan, W.Q. Zhang, Q.J. Wang, X.N. Zhao, A.D. Li, Z.G. Liu, M.W. Bayes, K.W. Yee., Scripta. Mat., 58, 2008, 65.
51. T. Frolov, Y. Mishin., Phy. Rev. Lett., 104, 2010, 055701.
52. I. Kaur, Y. Mishin, W. Gust. Fundamentals of Grain and Interphase Boundary Diffusion. Chichester, West Sussex: Wiley 1995.
53. JW. Cahn. Acta Metall 10, 1962, 789.
54. K. Lücke, H.P. Stüwe. In: Himmel L, editor, Recovery and Recrystallization of Metals. New York: Interscience Publishers, 1963; pp. 171–210.
55. M.I. Mendelev, D.J. Srolovitz. Model Simul Mater Sci Eng 10, 2002, R79